Structure–Mechanical Properties Relationship of Poly(ethylene terephthalate) Fibers

Milena Žiberna Šujica, Majda Sfiligoj Smole

University of Maribor, Faculty of Mechanical Engineering, Textile Department, Smetanova 17, SI- 2000 Maribor, Slovenia

Received 17 July 2002; accepted 26 December 2002

ABSTRACT: The correlation between the fiber structure and mechanical properties of two different poly(ethylene terephthalate) fiber types, that is, wool and cotton types produced by three producers, was studied. Fiber structure was determined using different analytical methods. Significant differences in the suprastructure of both types of conventional textile fibers were observed, although some slight variations in the structure existed between those fibers of the same type provided by different producers. A better-developed crystalline structure composed of bigger, more perfect, and more axially oriented crystallites was characterized for the cotton types of PET fibers. Crystallinity is higher, long periods are longer, and amorphous domains inside the long period cover bigger parts in this fiber type in comparison with the wool types of fibers. In addition, amorphous and average molecular orientation is higher. The better mechanical properties of cotton PET fiber types, as demonstrated by a higher breaking tenacity and modulus accompanied by a lower breaking elongation, are due to the observed structural characteristics. © 2003 Wiley Periodicals, Inc. J Appl Polym Sci 89: 3383–3389, 2003

Key words: fibers; mechanical properties; structure-properties relations

INTRODUCTION

The conventional spinning and drawing process of commercial poly(ethylene terephthalate) (PET) textile fibers involves the extrusion of the PET melt and winding-up at a speed of 500–1500 m min^{-1}.[1] The yarns produced by low-spinning processes are noncrystalline and only very slightly oriented [low-oriented yarns (LOY)].[1] The birefringence is less than 0.01 at a windup speed below 1500 m min^{-1}.[2] The resulting undrawn yarn (UDY) is then drawn three to five times and heat-treated to give the fully oriented yarn or drawn yarn (DY).[3]

Drawing is an essential fabrication process to achieve well-oriented structures with appropriate mechanical properties. The mechanical and/or thermal treatments result in the transformation of the isotropic structure into a fibrillar one.[4] Extraordinarily large-chain orientations, which are desired to increase material stiffness, can be obtained by applying a multistep drawing procedure with passing through an oriented and noncrystalline intermediate structure.[5] It is still difficult, however, to produce high-modulus and high-strength materials owing to the low deformability of PET.[6]

Correspondence to: M. S. Smole (majda.sfiligoj@uni-mb.si).

Journal of Applied Polymer Science, Vol. 89, 3383–3389 (2003)

The process of drawing using conventional spinning at conventional draw ratios introduces some crystallinity into the yarn, but is insufficient to stabilize the yarn against thermal shrinkage during further processing and use. It is therefore usual in filament yarn production to crystallize the yarn further by setting it during the drawing process through passage over a hot plate at a temperature within the range 140–220°C or by using a heated draw roller at similar temperatures.[2]

Even though there is a substantial use of polyester staple fiber in an unblended form, a much higher proportion is blended with other fibers to produce yarns, which benefit from the properties of each component. The type of staple fiber used is adjusted in terms of the diameter, length, and physical properties of the individual fibers to suit the particular blend. In the cotton system, the fibers usually used are 38 mm in length and their fines are 1.3 and 1.7 dtex, respectively. The polyester processed, either 100% pure or blended with wool, is usually in the range of 3.6–6.7 dtex and its staple length is about 58 mm.[2] Much research has been focused on the determination of quantitative structure–property relationships for predicting the performance of fibers, (e.g., refs. 7–11), but there is currently no exact study available on the differences between the structure and properties of the wool and cotton types of PET fibers. The aim of this present article was a detailed study of the structure–properties relationships of several commercial PET fibers of dif-

ferent origins of wool and cotton types and to compare both types of PET fibers.

EXPERIMENTAL

Materials

Different kinds of commercial PET staple fibers of wool and cotton types were studied. Cotton types (c) of different provenances with lengths of 38 mm and fineness varying between 1.5 and 1.7 dtex are marked I_c, II_c, and III_c. The wool types of PET fibers (w) were obtained from the same fiber producers (I, II, III) and they are marked I_w, II_w, and III_w . Fibers lengths are 75 and 90 mm, respectively, and their fineness, 3.3 dtex. PET polymer was produced after two different polycondensation processes. Fibers from producer II were synthesized from dimethyl terephtahalate and ethylene glycol. The process of fiber formation was continuous and drawing was performed in one step for the wool types of fibers and in two steps to achieve higher tenacity for cotton fiber types. Details of the production conditions were unavailable for the fibers produced by the first producer. Fibers from the third producer were synthesized from terephthalic acid and ethylene glycol in a discontinuous process.

Methods

Different analytical methods were used such as X-ray analyses, calorimetric measurements, density measurements, acoustic measurements, and birefringence determination for evaluation of the structural parameters. These methods are described in detail in refs. 11–16.

Detection of wide-angle X-ray scattering (WAXS) was performed using a flat-film camera and a Siemens D 500 diffractometer installed on a Kristallofleks 805 X-ray tube. Distribution of WAXS was followed on the equator where three interference reflections were observed of the (100), ($1\bar{1}0$), and (010) paratrope plains. Additionally, an amorphous sample with the density of 1.335 g cm^{-3} was measured. These measurements were performed over a scattering angle between $2\theta = 10^0$ and $2\theta = 35^0$. Additionally, the azimuthal scanning of the meridional ($\bar{1}05$) reflection was carried out to determine the crystalline orientation.

To separate the equatorial scattered intensities on the crystalline and amorphous parts, the Killian method[15] was used, as only a relative relationship between the different fiber types was of interest although several other more precise techniques were proposed (e.g., refs. 17–19). After inserting the measured amorphous background into the experimental scattering curve, the interference reflections of (100), ($1\bar{1}0$), and (010) planes were separated. For the individual crystalline profiles, the Gauss distribution was used for the

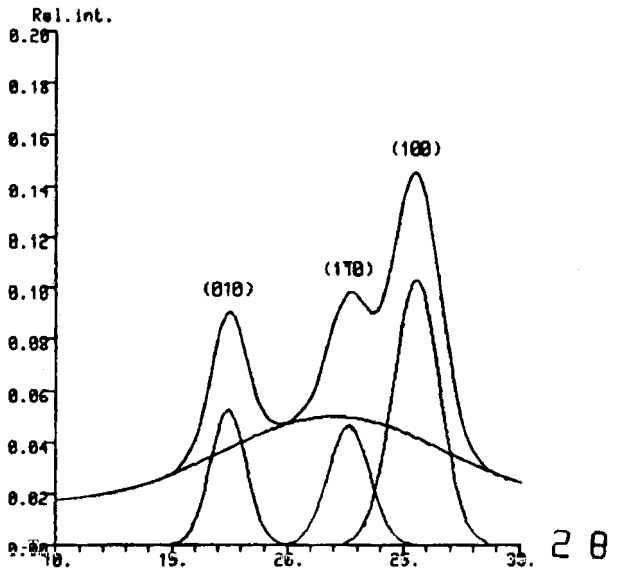

Figure 1 Equatorial WAXS curve with inserted amorphous background and separation of the crystalline and amorphous scattering (sample I_c).

approximation. The procedure is demonstrated in Figure 1 and was described in detail in refs. 11 and 12.

The crystallinity determined from the X-ray scattering $\alpha_{X\text{-ray}}$ is given by the ratio of the integrated intensities of the scattering of the equatorial reflections and the total coherent scattering, according to eq. (1)[14,15]:

$$\alpha_{X\text{-ray}} = \frac{\int_{2\theta_1}^{2\theta_2} I_c(\theta)d\theta}{\int_{2\theta_1}^{2\theta_2} I(\theta)d\theta} \quad (1)$$

I is the entire coherently scattered intensity; I_c, the coherent intensity present in the crystalline peaks; and 2θ, the diffraction angle.

The dimensions of crystallites perpendicular to the fiber axis, $\Lambda^*_{(100)}$, $\Lambda^*_{(1\bar{1}0)}$, and $\Lambda^*_{(010)}$, were determined from the half-width of the equatorial reflections using the Scherrer equation :

$$\Lambda^*_{(hkl)} = \frac{K\lambda}{\beta_{(hkl)}\cos\theta} \quad (2)$$

where K is the Scherrer constant; λ, the applied wavelength (0.1542 nm); β, the half-width of the reflection; and θ_{hkl}, the scattering angle of the (hkl) crystalline planes. The orientation function of the crystallites f_c defined by Hermans' equation was determined from the diffraction curves of the submeridional ($\bar{1}05$) reflection.[12,15] The separation of the submeridional ($\bar{1}05$) reflection is demonstrated in Figure 2:

$$f_c = \frac{1}{2}\left|3\overline{(\cos^2\tau)} - 1\right| \quad (3)$$
$$\cos\sigma \approx \cos\tau$$

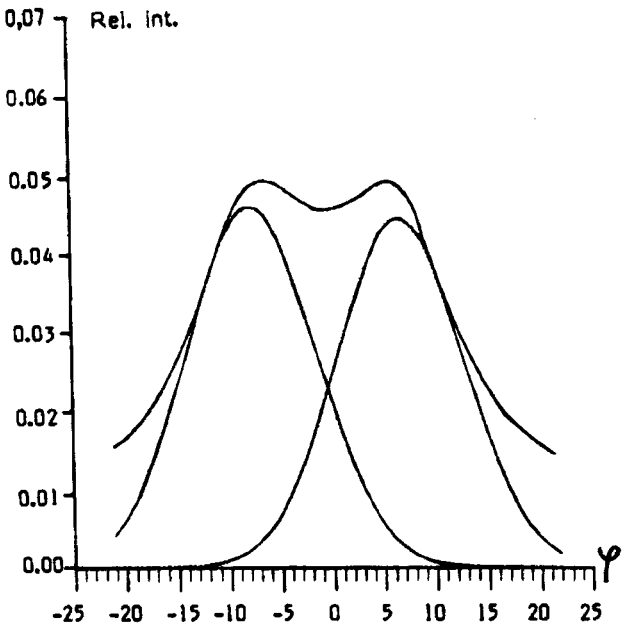

Figure 2 Meridional WAXS intensity curve of a PET fiber (sample II_c); separation of the submeridional ($\bar{1}05$) reflection.

$\cos \sigma \approx \cos \tau$. τ is the average angle of the crystallites' tilt according to the fiber axis, and σ, the half-width of the ($\bar{1}05$) reflection.

Small-angle X-ray scattering (SAXS) led to some information about the periodical fiber structure parallel to the fiber axis. SAXS was registered by a Kiessig film camera. The long spacing L, the dimensions of the crystallites parallel to the fiber axis D, and the length of the amorphous part of the fiber were determined from SAXS photographs. Long spacing, which is defined as the average repeating distance between the center of two crystallites, was determined directly by measuring the distance between the meridional reflection and the primary beam. The calculation of the long spacing followed Bragg's law [14,15]:

$$L = \frac{\lambda l_p}{A} \tag{4}$$

λ is the wave length of the X-ray beam (0.1542 nm); l_p the distance between the sample and the film (400 mm); and A, the mean measurement value of the meridional reflection/primary beam distance.

The length of the crystallites parallel to the fiber axis D is defined by the ratio among the long spacing, crystallinity index $\alpha_{\text{X-ray}}$, sample density ρ_s, and density of the crystalline phase ρ_c:

$$D = \frac{L\alpha_{\text{X-ray}}\rho_s}{\rho_c} \tag{5}$$

L is the long spacing (nm); $\alpha_{\text{X-ray}}$, the crystallinity index determined from X-ray scattering; ρ_s, the sample density (g cm^{-3}); and ρ_c, the density of the PET crystalline phase (1.455 g cm^{-3}).

The length of the amorphous part inside the long spacing l represents the difference between the long spacing and the length of the crystallites:

$$l = L - D \text{ (nm)} \tag{6}$$

The floating method according to Juilfs[20] was used for fiber density determination. The measured values were used for the crystallinity α_ρ calculation [cf. eq. (7)]:

$$\alpha_\rho = \frac{\rho_c(\rho_s - \rho_a)}{\rho_s(\rho_c - \rho_a)} \tag{7}$$

ρ_c is the density of the crystalline PET (1.455 g cm^{-3})[21]; ρ_a, the density of the amorphous PET (1.335 g cm^{-3})[21]; and ρ_s, the density of the sample (g cm^{-3}).

DSC thermograms were obtained on a Perkin–Elmer 7 differential calorimeter and the crystallinity parameter was calculated from the measured melting enthalpies according to eq. (8):

$$\alpha_{\Delta H} = \frac{\Delta H_{\text{ms}}}{\Delta H_{\text{mc}}} \tag{8}$$

ΔH_{ms} is the melting enthalpy of the sample (J g^{-1}), and ΔH_{mc}, the melting enthalpy of the 100% crystalline PET (121.3 J g^{-1}).[22]

The acoustic modulus was determined from the acoustic impulse propagation in the longitudinal fiber direction using the Bergmann equation ($E_a = \rho\, c^2$)[23] and the average molecular orientation f_{ma} and the orientation of macromolecular chains in the amorphous phase f_{aa} were calculated [eqs.(10) and (11)]. The Morgan Dynamic Modulus Tester PPM-5R apparatus was used for the acoustic measurements. Equation (9) was involved for the average molecular orientation factor f_{ma}:

$$f_{\text{ma}} = 1 - \frac{E_n}{E_s} \tag{9}$$

f_{ma} is the average molecular orientation factor; E_n, the acoustic modulus for nonoriented PET (0.26×10^{10} Pa)[23]; and E_s, the acoustic modulus of the sample (Pa).

The orientation of macromolecular chains in the amorphous phase f_{aa} is defined by

$$f_{\text{aa}} = 1 - \frac{E_n}{E_a} \tag{10}$$

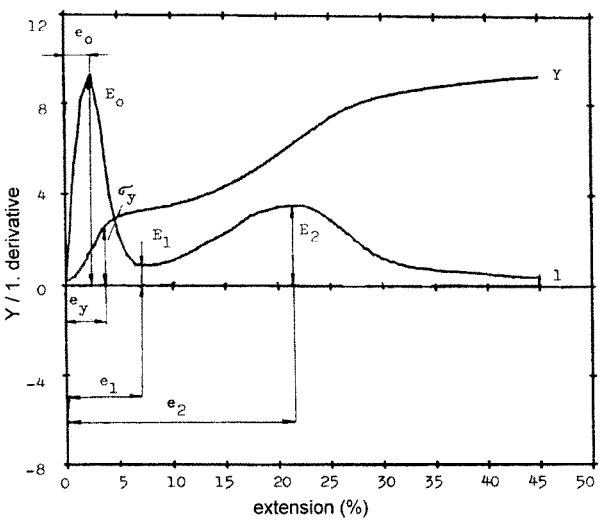

Figure 3 Method of the calculation and determination of the viscoelastic data of PET fibers: Y, stress–strain curve $\sigma = f(\varepsilon)$; 1, derivative of the experimental curve.

$$E_a = \frac{E_n(1 - \alpha_\rho)}{\frac{E_n}{E_s} - (1 - f_c)\alpha_\rho} \tag{11}$$

f_{aa} is the orientation factor of the amorphous phase; f_c, the orientation factor of the crystallites; E_a, the acoustic modulus of the amorphous PET (Pa); and α_ρ, the crystallinity index determined by the density measurements.

A compensation method according to Eringhaus was used for birefringence determination on a polarization microscope.[24] The average molecular orientation factor $f_{m\Delta n}$ and the amorphous orientation factor $f_{a\Delta n}$ were determined [cf. eqs. (12) and (13)] from these measurements:

$$f_{m\Delta n} = \frac{\Delta n_s}{\Delta n_{oi}} \frac{\rho_c}{\rho_s} \tag{12}$$

$f_{m\Delta n}$ is the average molecular orientation factor; Δn_s, the birefringence of the sample; Δn_{oi}, the birefringence of the ideally oriented PET (0.290 ± 0.009)[23]; ρ_c, the density of crystalline PET; and ρ_s, the density of the sample:

$$f_{a\Delta n} = \frac{\Delta n_s - \alpha_x f_c \Delta n_c^0}{(1 - \alpha_x)\Delta n_a^0} \tag{13}$$

$f_{a\Delta n}$ is the amorphous orientation factor; $\Delta^0{}_c$, the birefringence of the ideally oriented crystalline PET (0.220)[23]; and $\Delta^0{}_a$, the birefringence of the ideally oriented amorphous PET (0.275).[23]

Additionally, the mechanical properties of different PET fibers of both types were measured on an Instron 1122 dynamometer equipped with a data analyzer. The testing length was 10 mm, breaking was performed in 20 s, and the measurements of each sample were repeated 60 times. A mean curve was constructed from the measurements, and from there, some typical viscoelastic parameters were calculated and determined from the stress–strain curve, the integral curve, and the 1, 2, and 3 derivatives of the experimental curves (σ', σ'', σ'''), respectively, as shown in Figure 3. The elasticity modulus (E_0, E_1, E_2, E_3) with adequate extensions (ε_0, ε_1, ε_2, ε_3) was determined at the gradation points of the 1 derivative curve, where the 2 derivative curve crosses the x–axis. The yield point (σ_y, ε_y) was determined on the first derivative curve at the position of $\sigma''' = 0$. The work to rupture represents the area under the stress–strain curve and was determined by the integration of the experimental curve.[25]

RESULTS

The structural parameters of two different types, that is, cotton and wool types of PET fibers calculated from diffraction patterns, are collected in Tables I and II. The cotton-type PET fibers' crystallinity index as determined from the X-ray intensity distribution is between 0.398 and 0.437, and for wool types, between 0.328 and 0.405, respectively, that is, an increased crystallinity index of about 20% is observed for cotton

TABLE I
Crystalline Structure of Different PET Fibers of Cotton Type (Samples I_c, II_c, III_c)

Parameter	I_c cotton type	II_c cotton type	III_c cotton type
$\alpha_{X\text{-ray}}$	0.425	0.398	0.437
α_ρ	0.395	0.382	0.463
α_{DSC}	0.353	0.336	0.329
Long spacing L (10^{-1} nm)	110.0	107.5	116.0
Crystallites length D (10^{-1} nm)	44.3	40.5	48.4
Length of amorphous domain l (10^{-1} nm)	65.7	67.0	67.6
l/D ratio	1.48	1.65	1.4
Apparent crystallite size $\Lambda^*_{(100)}$ (10^{-1} nm)	38.50	33.69	41.80
Apparent crystallite size $\Lambda^*_{(1\bar{1}0)}$ (10^{-1} nm)	43.08	40.99	49.06
Apparent crystallite size $\Lambda^*_{(010)}$ (10^{-1} nm)	49.41	42.77	55.56

TABLE II
Crystalline Structure of Different PET Fibers of Wool Type (Samples I_w, II_w, III_w)

Parameter	I_w wool type	II_w wool type	III_w wool type
$\alpha_{X\text{-ray}}$	0.389	0.328	0.405
α_ρ	0.442	0.446	0.450
α_{DSC}	0.345	0.340	0.330
Long spacing L (10^{-1} nm)	93.7	87.2	96.6
Crystallites length D (10^{-1} nm)	34.7	31.7	37.3
Length of amorphous domain l (10^{-1} nm)	59.0	55.5	59.3
l/D ratio	1.7	1.75	1.59
Apparent crystallite size $\Lambda^*_{(100)}$ (10^{-1} nm)	38.77	33.37	40.65
Apparent crystallite size $\Lambda^*_{(1\bar{1}0)}$ (10^{-1} nm)	43.74	38.51	46.89
Apparent crystallite size $\Lambda^*_{(010)}$ (10^{-1} nm)	47.93	38.76	37.14

types in comparison to the wool types of PET fibers (Table I). The most crystalline fiber is the cotton type PET fiber III_c with a crystallinity index of 0.437 and the lowest crystallinity was found in the II_c fiber. Similar findings are characteristic for the wool types. There are some differences between the crystallinity index determined from X-ray measurements and the crystallinity index determined by density measurements, that is, for cotton types, the crystallinity determined from X-ray measurements is higher, and for wool types, the crystallinity determined by measuring the fiber density is higher. Nearly the same variations' tendency, however, is observed between fibers from different producers within the results of both determination techniques. Crystallinity determined from calorimetric measurements ranges from 0.329 to 0.353 for cotton types and from 0.330 to 0.345 for wool types. Crystallinity determined by the DSC method is lower than is the crystallinity obtained by the other two methods. Unexpectedly, low α_{DSC} crystallinity is observed for sample III in both groups when compared to the results obtained by X-ray scattering and density measurement, that is, these two samples show the highest crystallinity α_x and α_ρ indices (Tables I and II).

Long spacing, consisting of about 60% of the amorphous domains, is larger in the case of cotton PET fiber types (for cotton types, it is from 10.7 to 11.6 nm, and for wool types, from 8.7 to 9.7 nm). In both groups of fibers, the greatest long period is detected for fibers marked with III. The ratio l/D was used to study the structure of the long period. It represents the relationship between the lengths of amorphous and crystalline domains in the fiber fibrillar structure. A ratio of about 1.7 was determined for the wool-type PET fibers and a lower one (about 1.5) for cotton-type PET fibers.

There are some common structural characteristics in regard to the fiber producer. Fibers of both types marked with III have a higher crystallinity index, a greater long period, and a lower ratio between l/D and they are formed of larger crystallites.

Average molecular orientation, orientation of the crystallites, and orientation of the amorphous molecular segments are given in Tables III and IV. Crystalline orientation in cotton types of PET fibers is higher compared to the wool types. In the group of cotton types, the fibers from the first (I_c) and the third (III_c) producers have nearly the same crystalline orientation functions (0.935) and are higher than the crystalline orientation of the second sample (II_c) (0.907). Crystalline orientation varies much more between the PET fibers of the wool types. Lower average molecular orientations were observed when calculated from the measured birefringence of the fibers in comparison to the values obtained by measuring the acoustic impulse propagation through the fiber sample. There are no significant differences between the average molecular orientations in fibers from different groups. A higher amorphous orientation is determined for fibers of the cotton type using both methods. PET fiber of the wool type from the first producer (I_w) differs from others because of the very low average orientation and amorphous orientation but with a rather high crystalline orientation function.

The mechanical properties are collected in Tables V and VI and are graphically represented in Figure 4. A steep and a rather short load–elongation curve is ob-

TABLE III
Orientation Parameters of Different PET Fibers of Cotton Type (Samples I_c, II_c, and III_c)

Parameter	I_c cotton type	II_c cotton type	III_c cotton type
Crystalline orientation factor f_c	0.936	0.907	0.935
Average molecular orientation factor $f_{m\Delta n}$	0.562	0.573	0.561
Average molecular orientation factor f_{ma}	0.779	0.779	0.808
Amorphous orientation factor $f_{a\Delta n}$	0.425	0.471	0.423
Amorphous orientation factor f_{aa}	0.739	0.757	0.731

TABLE IV
Orientation Parameters of Different PET Fibers of Wool Type (Samples I_w, II_w, and III_w)

Parameter	I_w wool type	II_w wool type	III_w wool type
Crystalline orientation factor f_c	0.927	0.832	0.901
Average molecular orientation factor $f_{m\Delta n}$	0.517	0.519	0.561
Average molecular orientation factor f_{ma}	0.681	0.683	0.790
Amorphous orientation factor $f_{a\Delta n}$	0.344	0.406	0.435
Amorphous orientation factor f_{aa}	0.486	0.564	0.699

served for the cotton type of PET fibers. Extension suddenly becomes much easier after a rather long initial period with a steep slope. In this region, the yield point occurs and fiber deformation is not facilitated until a relative high load and breaking occurs at a breaking extension of between 35 and 55%. A high modulus E_1 and E_2 with a low elongation at these points was determined for the analyzed cotton types of fibers as the initial modulus is equal to the slope of the stress–strain curve at the origin. The curves of the wool types already show a lower curve slope in the elastic domain, having a lower tenacity at the yield point and a higher extensibility than those of the cotton types. They are somehow softer after the yield point, which means that, for deformation, a low load is needed, and after the strenghtening domain, breaking occurs at a lower load but with a higher breaking extension compared to the cotton variety.

The curve σ/ε for fibers I_c and III_c are typical for the cotton type of PET fibers, while sample II_c shows some characteristics of the wool PET fibers. In the wool-type group of analyzed fibers, an exemption is represented by sample I_w, with the tenacity–extension curve being very similar to a typical curve for the cotton types of PET fibers.

Steep tenacity–extension curves, higher breaking tenacities accompanied by lower breaking extensions, and higher moduli of the cotton types of fiber are due to the higher crystallinity and orientation, especially amorphous orientation of these types of PET fibers. The breaking tenacity of fiber II_c is even higher than is the tenacity of the other two fibers in the cotton-type group. This is due to the high orientation of the amorphous domains in spite of a rather low crystallinity and a low average molecular orientation leading to unsuitable other viscoelastic parameters. The high breaking tenacity of fiber I_w arises from the high fiber crystallinity. The results are in a good correlation with structure–property relationship observed for other fiber types.[13,23, 26–30]

CONCLUSIONS

In this article, the structural–property correlation for cotton and wool types of PET fibers was studied. Fine structure parameters significantly differ between these two types of PET fibers, although some differences also exist in groups of the same fiber types.

The higher density of the PET cotton fiber types arises from a higher crystalline and more oriented structure. The long periods in the cotton-type fibers are longer but the dimensions of the crystallites are very similar to the wool types. The cotton types of PET fibers are more rigid, due to these structural differences, which are confirmed by higher initial moduli, lower elongations, and the slopes of the tenacity–elongation curves, which are more precipitous. A slightly higher glass transition temperature is observed for this fiber type and the relaxation shrinkage is in correlation with the amorphous orientation. Comparing

TABLE V
Mechanical Properties of Different PET Fibers of Cotton Type (Samples I_c, II_c, and III_c)

Property	I_c	II_c	III_c
Tenacity σ_B (cN/tex)	51.7	54.9	53.6
Breaking extension ε_B (%)	35.4	55.2	46.4
Initial modulus E_0 (GPa)	3.64	3.41	3.25
Deformation ε_0 (%)	3.50	2.40	2.80
Modulus E_1 (GPa)	2.75	1.27	2.45
Deformation ε_1 (%)	5.50	7.70	6.00
Modulus E_2 (GPa)	4.58	3.02	4.03
Deformation ε_2 (%)	12.50	20.20	13.00
Modulus E_3 (GPa)	−0.67	−1.36	−0.53
Deformation ε_3 (%)	4.0	3.5	4.3
Yield stress σ_y (cN/tex)	10.20	8.39	9.56
Yield strain ε_y (%)	4.2	3.67	4.40
Work to rupture A_B (mJ)	0.30	0.23	0.25

TABLE VI
Mechanical Properties of Different PET Fibers of Wool Type (Samples I_w, II_w, and III_w)

Property	I_w	II_w	III_w
Tenacity σ_B (cN/tex)	44.6	41.6	41.0
Breaking extension ε_B (%)	61.6	69.2	66.1
Initial modulus E_0 (GPa)	3.34	2.18	2.49
Deformation ε_0 (%)	2.75	4.00	3.00
Modulus E_1 (GPa)	1.26	0.43	0.24
Deformation ε_1 (%)	6.70	10.00	11.00
Modulus E_2 (GPa)	4.20	1.73	2.04
Deformation ε_2 (%)	12.10	29.00	23.00
Modulus E_3 (GPa)	−0.81	−0.48	−0.36
Deformation ε_3 (%)	4.4	6.0	5.0
Yield stress σ_y (cN/tex)	10.24	7.30	11.10
Yield strain ε_y (%)	4.38	5.97	8.09
Work to rupture A_B (mJ)	0.59	0.67	0.65

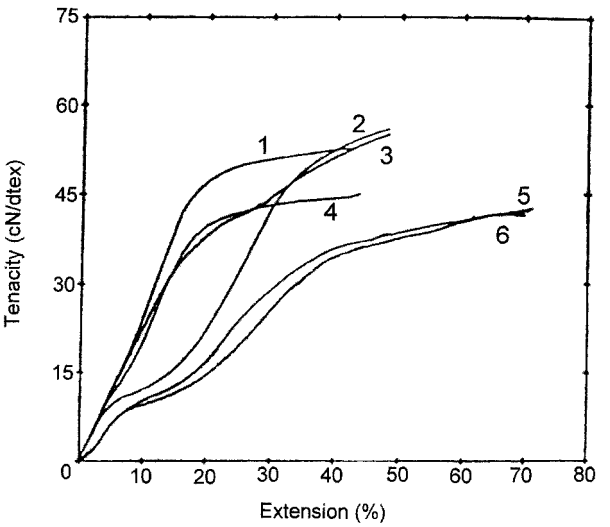

Figure 4 Mechanical properties of PET fibers of cotton and wool types of different origins: (1) I_c; (2) II_c; (3) III_c; (4) I_w; (5) II_w; (6) III_w.

the structural parameters of fibers from different origin fibers from producer II show a not so well developed fibrillar structure compared to that of the other two fibers from producers I and III and they differ according to their response to the mechanical forces. Fibers are softer and they have higher breaking elongation accompanied by higher tenacity.

Greater structural differences were observed in the wool-type fibers' group. The fibers differ significantly in crystalline and amorphous orientation, which is in correlation with the relaxation shrinkage and glass transition temperature, but not as clearly confirmed by the viscoelastic properties.

The observed differences in the fiber fine structure and the properties are due to the different conditions prevailing during fiber production. The fiber-production process of producer III enables formation of bigger, more highly oriented crystalline structures which are too stiff for conventional textile requirements. In contrast, fibers from producer II possess a structure that is not developed enough, the crystallites are smaller and defective with a lower orientation, and the fibers are too extensive when compared to the others.

References

1. Rodriguez Cabello, J. C.; Santos, J.; Merino, J. C.; Pastor, J. M. J Polym Sci Part B Polym Phys 1996, 34, 1243.
2. McIntyre, J. E. Polyester Fibers in Fiber Chemistry; Lewin; M.; Pearce, E. M., Ed.; Marcel Dekker: New York, 1985; Chapter 1.
3. Nakajima, T. Advanced Fiber Spinning Technology; Woodhead: Cambridge, 1994.
4. Fakirov, S.; Evtatiev, M. Polymer 1990, 31, 431.
5. Göschel, U. Polymer 1996, 37, 4049.
6. Huang, B.; Ito, M.; Kanamoto, T. Polymer 1994, 35, 1329.
7. Berg, H. Chem Text 1972, 215.
8. Fu, Y.; Annis, B.; Boller, A.; Jin, Y. J Polym Sci Part B Polym Phys 1994, 32, 2289.
9. Murthy, N. S.; Grubb, D. T.; Zero, K.; Nelson, C. J.; Chen, G. J Appl Polym Sci 1998, 70, 2527.
10. Šujica, M.; Malej, S.; Sfiligoj, M. Tekstilec 1989, 32, 246.
11. Šujica, M.Thesis, University of Ljubljana, 1988.
12. Golob, B.; Žiberna Šujica, M.; Stjepanovič, Z. Informatika 1990, 31, 59.
13. von Falkai, B. Synthesefasern; Verlag Chemie: Weinheim, 1981.
14. Bodor, G. Structural Investigation of Polymers; Ellis Horwood: New York, London, 1991.
15. Alexander, L. E. X-ray Diffraction Methods in Polymer Science; Wiley-Interscience: New York, 1985.
16. Sfiligoj Smole, M.; Zipper, P. Colloid Polym Sci 1999, 276.
17. Murthy, N. S.; Correale, S. T.; Minor, H. Macromolecules 1991, 24, 1185.
18. Murthy, N. S.; Bednarczyk, C.; Rim, P. B.; Nelson, C. J. J Appl Polym Sci 1997, 67, 1363.
19. Murthy, N. S. Polym News 1991, 16, 358.
20. Juilfs, J. Melliand Text 1959, 40, 1136.
21. De, R.; Daubeny, P.; Bunn, C. W.; Brown, C. J. Proc R Soc A 1954, 226, 531.
22. Roberts, R. C. Polymer 1969, 10, 113; Polymer Handbook, 2nd ed.; Brandrup, J.; Immergut, E. H., Ed.; Wiley-Intersecience: New York, London, Sydney, Toronto, 1975.
23. Samuels, R. J. Structured Polmer Properties, Wiley-Interscience: New York, 1974.
24. Nettelnsroth, K. Melliand Text 1972, 53, 727.
25. Bukošek, V. Tekstilec 1983, 26, 24.
26. Sfiligoj Smole, M.; Doleček, V.; Žiberna Šujica, M. DWI Rep 1993, 111, 653.
27. Žiberna Šujica, M. In Proceedings of the International Symposium on Novelties in Textiles, Ljubljana, 1990; p 56.
28. Žiberna Šujica, M.; Malej, S.; Sfiligoj, M. Tekstilec 1986, 29, 83.
29. Fisher, E. W.; Fakirov, S. J Mater Sci 1976, 11, 1041.
30. Prevoršek, D. C.; Butler, H. R.; Knows, Y. D.; Lamb, G. E. R.; Sharma, R. K. Text Res J 1977, 47, 107.